J. Fluid Mech. (2012), *vol.* 710, *pp.* 482–504.
doi:10.1017/jfm.2012.374

Direct numerical simulation of axisymmetric wakes embedded in turbulence

Elad Rind‡ and Ian P. Castro†

Aeronautics, Faculty of Engineering and the Environment, University of Southampton, Southampton SO17 1BJ, UK

(Received 10 January 2012; revised 17 July 2012; accepted 19 July 2012; first published online 29 August 2012)

Direct numerical simulation has been used to study the effects of external turbulence on axisymmetric wakes. In the absence of such turbulence, the time-developing axially homogeneous wake is found to have the self-similar properties expected whereas, in the absence of the wake, the turbulence fields had properties similar to Saffman-type turbulence. Merging of the two flows was undertaken for three different levels of external turbulence (relative to the wake strength) and it is shown that the presence of the external turbulence enhances the decay rate of the wake, with the new decay rates increasing with the relative strength of the initial external turbulence. The external turbulence is found to destroy any possibility of self-similarity within the developing wake, causing a significant transformation in the latter as it gradually evolves towards the former.

Key words: shear flow turbulence, turbulence simulation, wakes

1. Introduction

Axisymmetric turbulent wakes have been studied for over half a century, not least because in the far field (when the maximum wake deficit velocity, U_s, is small in comparison to the free-stream velocity, U_∞) they are one of the classical free shear flows for which the equations of motion suggest the possibility of self-similar behaviour. This was famously clarified by Townsend (1976) and numerous experiments have been conducted which confirm such behaviour. However, recent authors have suggested that the universal self-similarity hypothesis is false (as explained in the historical review of Johansson, George & Gourlay 2003). In particular, it has been argued that the asymptotic structure of such self-preserving wakes (just as for other related flows) is perhaps not independent of initial conditions. Indeed, such independence seems unnecessary for self-similar solutions to appear. This was perhaps first illustrated by the measurements of Bevilaqua & Lykoudis (1978), whose data obtained in wakes behind bodies differing in character but having the same drag coefficient showed that the wakes reached different states of similarity. Wygnanski, Champagne & Marasli (1986) subsequently undertook a similar and even more convincing experiment of the same kind, but for planar wakes, reaching essentially the same conclusions. Johansson *et al.* (2003), following George (1989), provided a

† Email address for correspondence: i.castro@soton.ac.uk

‡ Current address: Department of Mechanical Engineering, University of Ottawa, ON, K1N 6N5, Canada.

'proper equilibrium similarity analysis', which demonstrated, as did their experiments on an axisymmetric wake, that initial conditions (and local Reynolds number) dominate the asymptotic behaviour. Although the effects of initial conditions do not appear in the appropriately normalized velocity profiles, they certainly do in growth rate and higher velocity moments.

A further major conclusion of the more recent work in the context of spatially developing, fully turbulent axisymmetric wakes is that there are two possible self-similar scalings for the far-field behaviour (i.e when $U_s/U_\infty \ll 1$). Each has $\delta \propto x^n$ and $U_s \propto x^{-2n}$, where δ is a typical wake length scale, e.g. the half-width (defined throughout this paper in the usual way as twice the value of the radial coordinate r where the mean velocity deficit is half its maximum value). The first possibility is the classical result that $n = 1/3$, valid when viscous effects can be ignored, i.e. at asymptotically large Reynolds numbers. The second has $n = 1/2$, which appears from the analysis of the momentum equation when viscous terms are included, provided either that the turbulent stresses are identically zero (the purely laminar wake originally analysed by Batchelor 1967), or that the turbulence stress term is of the same order as the viscous term. If the former is of greater order than the latter, the $n = 1/2$ solution can also appear if either the radial variations of turbulent and viscous stresses are identical or the eddy viscosity is constant with x. It is not easy to identify which scaling appears in experiments, whether numerical or physical, but Johansson *et al.* (2003) claim that both have done so. However, as Redford, Castro & Coleman (2012) have recently demonstrated, even after extremely long times (or, equivalently, spatial distances) the turbulent wake retains relatively large turbulent stresses (cf. the laminar ones), so it seems that the $n = 1/2$ solution for a turbulent wake can only properly occur under either of the restrictive conditions mentioned above. A fully turbulent wake might not asymptotically become genuinely laminar, as indeed Johansson *et al.* (2003) suggested, but proof of this would require full consideration of all the higher-order transport equations; the transition from the long-time universal $n = 1/3$ turbulent state identified by Redford *et al.* (2012) to the very final state has never been fully explored.

In recent years there have been a few direct numerical simulations (DNS) of the time-dependent analogue of spatially developing wakes. Moser, Rogers & Ewing (1998) studied planar wakes, and undertook a similarity analysis in the spirit of George (1989), whereas Gourlay *et al.* (2001) considered the axisymmetric wake, a flow very recently re-visited by Redford *et al.* (2012) specifically in order to demonstrate the effect of initial conditions and explore the possible consequent non-universality of such wakes. Although there are some fundamental differences between a time-dependent, axially homogeneous flow and the time-independent, spatially developing flow (as discussed by Redford *et al.* 2012), there is no reason to suppose any fundamental differences in their long-lived dependence on initial conditions. These various computations at first sight reinforce the above conclusions about dependence on initial conditions derived from studies on spatially developing wakes. However, Redford *et al.* (2012) conclude that such dependence is simply a result of the lack of sufficient time (or space) development; a truly universal wake structure (i.e. independent of initial conditions) does eventually appear but (in the spatial case) not before a distance downstream equal to at least 40 000 initial wake diameters – so far as to be unlikely ever to appear in real situations.

In practice many axisymmetric wakes develop in the presence of free-stream turbulence. Examples include submarine and wind turbine wakes, where the external turbulence may not decay on time or length scales similar to those of the wake decay, and turbine blade wakes, where it presumably does. Provided it is strictly of

an isotropic, homogeneous type (i.e. contains no Reynolds shear stress) the presence of such turbulence does not explicitly affect the similarity analyses – at least as far as the momentum equations are concerned. But it is intuitively clear that it must affect the way in which the wake decays, to an extent which is likely to depend on a number of governing parameters. Suppose that the external fully developed homogeneous isotropic turbulence (HIT) can be 'switched on' once the wake has reached its self-similar state and has an initial turbulence level characterized by an r.m.s. velocity fluctuation u'_{eo} and an integral length scale of L_{eo}. Arguably the most important of the governing parameters are u'_{eo}/U_{so} and L_{eo}/δ_o, where U_{so} and δ_o are the maximum wake deficit velocity and the wake half-width, respectively, at the time the free-stream turbulence appears. Of course, this is a somewhat idealized situation which could never be produced experimentally. Note that throughout this paper suffix 'e' refers to conditions in the external turbulence and suffix 'o' to initial conditions – at the time when the two fully developed flows are combined.

It appears that Wu & Feath (1994) were the first to conduct measurements of a wake in turbulent environments. They used a sphere as the wake generator and, inevitably, the free-stream turbulence was present during the initial formation and development of the wake as well as further downstream. The ambient turbulence intensity u'_e/U_∞ (at the location of the wake-generating body) was 4 % and the sphere Reynolds number was in the low to moderate range ($125 < Re_d = U_\infty d/\nu < 1560$, where d is the sphere diameter and U_∞ is an appropriate reference velocity). The free-stream turbulence was generated using a turbulent pipe flow and the sphere was mounted at the downstream end of the pipe. In comparison with non-turbulent environments (and high-Reynolds-number conditions) Wu & Feath found a decay rate governed by $n = 1/2$, which they noted is like a self-preserving laminar wake. They later studied the effect of different ambient turbulence intensities, 2–9.5 %, on the sphere wake at similar Reynolds numbers (Wu & Feath 1995). This time, each different ambient turbulence intensity was generated in a different way and they found a final decay region, beginning when the wake centreline turbulence intensity was approximately equal to the ambient one, in which decay rates faster that $n = 1/2$ were noticed, although no quantitative values were given. They also found some cases in which vortex shedding from the sphere had significant effects. Similar studies were undertaken by Legendre, Merle & Magnaudet (2006), who used large-eddy simulation (LES) to compute the wakes of a spherical bubble and of a solid sphere in a turbulent pipe flow. They also found a faster decay rate regime once the r.m.s. velocity in the free stream was of the same order as that on the wake centreline. The wakes of small particles in isotropic turbulence have also been studied using DNS (Bagchi & Balachandar 2003, 2004). In this case the turbulence integral scale was very large compared with the particle diameter (because the application was typical two-phase flows).

Recently studies of sphere wakes in roughly HIT have been reported (Amoura *et al.* 2010), for $110 < Re_d < 1080$. These were in some senses less complex cases than some of the earlier experiments mentioned above, in that there was no mean velocity shear outside the wake, and the turbulence there was approximately both homogeneous and isotropic. On the other hand, Re_d was sufficiently small to mean that their various cases covered only the laminar and transitional regimes for their pure-wake base cases. They also used external turbulent fields with very high turbulence intensities ($0.17 < u'_e/U_\infty < 0.26$) and integral scales some 3–4 times the sphere diameter, so

Authors	Methodology	Re_d	u'_e/U_∞	L_e/d	Re_{λ_e}	n
WF	Expt (pipe)	125–1560	0.02–0.095	8–59	—	$\geqslant\frac{1}{2}$
LMM	LES (pipe)	200	0.021	7.69	—	$\geqslant\frac{1}{3}\rightarrow 1$
BB	DNS (free)	58–610	0.06–0.15	52.6–333.3	164	$\frac{1}{2}$
ARRB	Expt (free)	110–1080	0.17–0.26	2.9–3.9	—	1
Present	DNS (free)	$>10\,000$	$\approx$0.022–0.087	$\approx$3.6–5.3	133–314	$\frac{1}{3}\rightarrow\frac{1}{2}$

TABLE 1. Wake decay law found (n) and defining parameters at the body location, of the different earlier works: WF, Wu & Feath (1994, 1995); LMM, Legendre *et al.* (2006); BB, Bagchi & Balachandar (2003, 2004); AARB, Amoura *et al.* (2010). 'Pipe' refers to experiments in which the wake-generating body was on the centreline of a developed turbulent pipe flow and 'free' refers to open flow conditions with (roughly) isotropic external turbulence. $Re_{\lambda_e}=u'_e\lambda_e/\nu$ is the microscale Reynolds number in the external flow. L is the (axial) integral scale, suffix 'e' denotes values in the external turbulence.

the turbulence remained (nearly) axially homogeneous over some $15d$ downstream of the sphere. They found an $n=1$ decay and, interestingly, that the wake scaled with the standard deviation of the eternal turbulence (u'_e) rather than the mean free-stream velocity (U_∞), but measurements only extended to $x/d=15$, i.e. not into the genuine far-wake region. We mention finally the work of Eames *et al.* (2011), who presented a theoretical analysis of sphere wakes in external turbulence. Although, when the external turbulence velocity is comparable with the centreline wake deficit, they found an $n=1$ decay, they only considered low-Reynolds-number cases, i.e. when there was no turbulence generation by the sphere itself. They specifically excluded consideration of the high-Reynolds-number fully turbulent cases like those studied here.

These various works clearly revealed that free-stream turbulence generally increases the wake decay rates, as might be expected. However, there are significant differences in the results, probably reflecting in the earlier cases the important influences of mean velocity shear in the free stream and possibly the constraining effects of pipe walls as the wakes grew and, in the later cases, the very different turbulence intensities and ratios of integral scale to body diameter. Table 1 lists the salient parameters from the various laboratory and numerical experiments. Notice that all these earlier sets of data were at relatively low Reynolds numbers and all but Amoura *et al.* (2010) had L_e/d ratios of $O(10)$ or higher. On the other hand, although the latter had L_e/d nearer $O(1)$ they had very high external turbulence levels. In an initial attempt to set up an experiment with fewer complications than those of Wu & Feath (1994, 1995) and Legendre *et al.* (2006), Redford & Coleman (2007) used DNS to model the time-dependent, axially homogeneous axisymmetric wake immersed in essentially isotropic but decaying free-stream turbulence. Like Gourlay *et al.* (2001) but unlike the later work of Bagchi & Balachandar (2003, 2004), they did not include the generating body. Unlike Gourlay *et al.*, however, they created an initial wake using a series of ring vortices, which with time broke and developed into an axisymmetric wake. This was then combined with the free-stream turbulence. Their main finding was that the stronger the free-stream turbulence, the more rapidly did the wake merge into its turbulent surroundings.

The present work is essentially a continuation of the Redford & Coleman (2007) study, using the same code but with different initial conditions and a range in the

governing parameters which covers intensities significantly smaller than those used by Amoura *et al.* (2010) but still with $O(1)$ values of L_e/d. Furthermore, the present work concentrates on the effect of the turbulence on the structure of the fully turbulent decaying far wake in situations where the external turbulence is also decaying (unlike the Amoura *et al.* 2010 case), as well as issues concerning wake decay rates and the possibility of self-similarity. Because the present methodology does not include a free-stream mean velocity, it is not straightforward to define either Re_d or u'_e/U_∞. Approximate values are included in table 1 (see later); note immediately that Re_d is much higher than in all earlier work, so typical velocity spectra in the present work contain clear inertial subranges with the classical $-5/3$ slope. Some corresponding experiments of the spatially developing analogue have also been conducted; these have been reported separately (Rind & Castro 2012).

Our work was motivated by interest in the development of the decaying wake in cases where the external turbulence decays simultaneously (unlike any other work). Furthermore, we initially speculated that if, for the spatially developing case, the external turbulence decays at about the same rate as the wake in the absence of external turbulence, then the wake in the presence of free-stream turbulence may not initially be strongly affected by the latter. Given that in at least some wind tunnel realizations of HIT u'_e/U_∞ has been reported to decay like $x^{-p/2}$ with $p \approx 1.3$ (but see § 3.2), whereas the (high-Reynolds-number) axisymmetric-wake maximum velocity deficit U_s/U_∞ decays like $x^{-2n} = x^{-0.67}$, the parameter u'_e/U_s may remain roughly constant. Likewise, with these decay power laws, it can be shown that the ratio of the free-stream-turbulence integral scale to the wake width L_e/δ may also be almost constant. Thus the lowest-order governing parameters for a wake immersed in free-stream turbulence might perhaps not change much along the wake, which might therefore initially have just the same decay behaviour as in the absence of external turbulence. DNS for isotropic turbulence typically shows decay rates similar to those found in wind tunnels, so one would anticipate analogous behaviour for the time-dependent spatially homogeneous case. It turns out that this expectation is not fulfilled except perhaps in the very weakest external turbulence fields; wake self-similarity rapidly collapses even with relatively weak external turbulence, as we will show.

The methodology is presented in § 2, followed by consideration of the separately computed wake and turbulent fields in § 3. Results and discussion for the combined flows are given in § 4 and conclusions are summarized in § 5.

2. Methodology

The use of DNS for any study of far-field wakes would be impossibly expensive if the wake-generating object were to be included. (Note that although the Bagchi & Balachandar 2003, 2004 DNS included the obstacle, it used a very restricted domain which did not extend beyond $15d$ downstream). We therefore followed Gourlay *et al.*'s (2001) and Redford & Coleman's (2007) less expensive approach – simulating the far-wake region only. The code was that used by Redford & Coleman (2007) and Redford *et al.* (2012); this is a triply periodic pseudo-spectral approach based on the method of Kim, Moin & Moser (1987). The simulation is thus of a time-developing, axially (and circumferentially) homogeneous flow with zero free-stream velocity which, as explained in Redford *et al.* (2012), maintains a time-invariant volume flux. Whether or not there is turbulence outside the wake, the volume flux deficit is $\dot{m} = -2\pi \int_{-\infty}^{\infty} Ur \, \mathrm{d}r$

so if the mean velocity field is self-similar (i.e. $U = U_s(t)f(\eta)$ where $\eta = r/\delta(t)$) then $\delta^2 U_s$ is time-invariant; r is the radial coordinate measured from the axis of symmetry (with x and θ the axial and circumferential coordinates, respectively). Note that in the spatially developing case, with a free-stream velocity of U_∞, U is the difference between U_∞ and the velocity in the wake, u_w say. But self-similarity in such a wake only occurs asymptotically for $U_\infty - u_w \ll U_\infty$; the constant-momentum constraint is then in fact equivalent to conservation of $\dot{m}$.

The specified initial condition for the wake mean velocity profile was extracted from experimental measurements of a spatially developing wake, just as Moser *et al.* (1998) did for their plane-wake DNS. Wake data reported by Chevray (1968) were used, with the reported mean velocity deficit profile at one disk diameter downstream scaled, while maintaining the profile shape, so that the wake initial Reynolds number Re, based on the half-width, δ, and the centreline deficit velocity, U_s, was 10 000. Note that with the assumption that this is equivalent to a spatially developing wake in a free stream such that the wake width and velocity deficit are similar to those found experimentally by Amoura *et al.* (2010) at $x/d \approx 10$, this is roughly equivalent to an obstacle Reynolds number Re_d well in excess of 10 000 – hence the entry in table 1. The scaled profile was then inserted into the computational domain with appropriate wake turbulence statistics superimposed using a modified version of Xie & Castro's (2008) digital filter. This essentially required specification of a random-number field, suitably filtered and correlated to ensure an initial integral length scale equal to the wake half-width. This is not consistent with a divergence-free field but, since continuity is immediately enforced by the code, the initial correction stage was quite short. The subsequent evolution towards the expected pure-wake structure was much longer, but still very short compared with the total computational time. Precise details of this evolution are immaterial (Redford *et al.* 2012) but depend on the details of the initial turbulence field. The eventual, self-similar wake discussed in § 3 has (at least) the expected first- and second-order properties, which would emerge independently of the initial conditions. Alternative methods might have marginally reduced the computational time required for this period of evolution, but were not tried. It is important to note that this wake, although self-similar, is not the eventual, universal self-similar state that is totally independent of initial conditions and only appears after extremely long computational times (Redford *et al.* 2012). But for the present purposes this does not matter; it is the effects of external turbulence on a genuinely self-similar wake that are of interest.

In addition to the wake, three HIT fields were generated separately. Recall that perhaps the major parameters affecting the wake development in a turbulent field include u'_{eo}/U_{so}, which we call the 'strength' of the free-stream turbulence (relative to the wake), and L_{eo}/δ_o, where u'_{eo} and L_{eo} are the r.m.s. velocity and integral length scale of the external turbulence at the time the latter is added outside the wake. The integral length scale is defined in the usual way as the area under the normalized spatial correlation Λ_x (defined by (2.1) below) of the axial velocity, up to the point where Λ_x is first zero. In order to achieve a specific turbulence strength a weaker field was generated first and prevented from decaying by using the forcing scheme of Sullivan, Mahalingam & Kerr (1994). Then, knowing the initial value of U_{so} from the preceding (pure) wake computation, the forcing constant (the turbulent kinetic energy) was increased gradually until the required u'_{eo}/U_{so} was achieved. Note that the integral length scale is actually only an output of the simulation and cannot be controlled

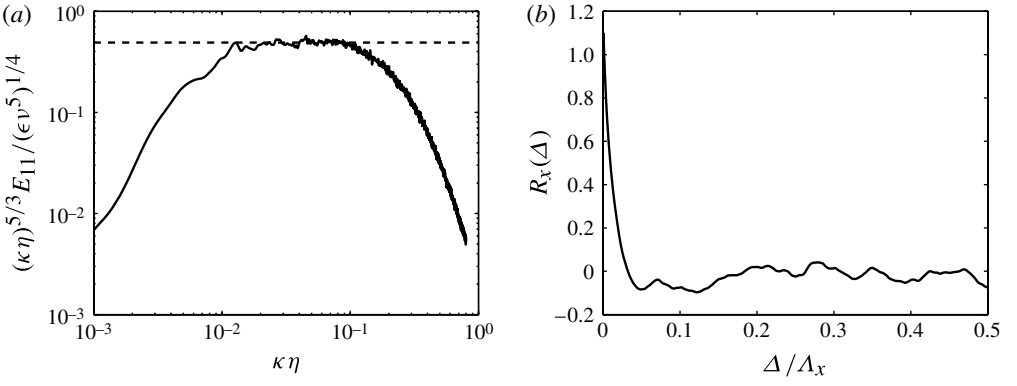

FIGURE 1. (*a*) A typical one-dimensional energy spectrum, E_{11}, at the wake half-width point. Solid line: the computed spectrum; dashed line: the universal inertial region value, C. (*b*) Example of the (axial velocity) spatial correlation function, $R_x(\Delta)$, at the wake half-width point; $3000 < Re < 4000$. $\Lambda_x/2L_x = 43$, where Λ_x is the axial length of the domain.

a priori. Also note that the forcing was only used during the development process and was removed immediately the turbulent field was added to the region outside the wake.

The domain for the wake simulations (both with and without external turbulence) was $4\pi \times 16\pi \times 4\pi$, with $512 \times 2048 \times 512$ Fourier modes. Each time step typically took 50 s when using 512 processors of the UK's HPCx facility. Since up to 40 000 time steps were required for the initial HIT simulations to achieve a stationary state (see § 3.2) a cheaper approach was required in order to reduce the computational cost. First the domain size was chosen to be $4\pi \times 4\pi \times 4\pi$, i.e. only one quarter the axial length of the wake domain. Moreover, for the first 95 % of those initial simulations the domain had only $256 \times 512 \times 256$ Fourier modes (with each time step typically taking 5 s when using 256 processors) and for the final 5 % it was increased to $512 \times 512 \times 512$ (with each time step typically requiring 21 s when using 256 processors). The code uses Cartesian coordinates and solutions were interpolated to the appropriate cylindrical coordinates using Press *et al.*'s (1992) two-dimensional interpolation. (Since the wake is axisymmetric and axially homogeneous, both circumferential and axial data averaging at fixed r was possible.)

In all computations, local Kolmogorov length scales, $\eta = (\nu^3/\epsilon)^{1/4}$, where ϵ is the mean local dissipation rate, varied between 20–110 % of the computational grid resolution. As an example of the satisfactory nature of both resolution and statistical convergence in all the simulations, figure 1(*a*) shows an axial kinetic energy (compensated) spectrum in the pure wake at $r = \delta$ averaged over times corresponding to $3000 < Re = U_s\delta/\nu < 4000$. The spectrum is compared with the universal result expected in the inertial subrange ($E_{11} = C\epsilon^{2/3}\kappa^{-5/3}$ where κ is the wavenumber and C is proportional to the Kolmogorov constant and has the value 0.49, e.g. Pope 2000). The spectral properties (i.e. E_{11} and ϵ, where E_{11} is the one-dimensional spectrum of the axial velocity) were directly calculated from the simulation data using the exact relationship, $\epsilon = 2\nu\overline{S_{ij}S_{ij}}$ where S_{ij} is the usual fluctuating strain rate tensor. The agreement is very satisfactory and it may be noted that a significant inertial subrange is present, where the compensated spectrum is constant, although recall that

Wang *et al.* (1996), among others, suggest that the Kolmogorov constant might be slightly larger than 0.49; small differences would not be apparent on such a plot.

As the wakes grow there will eventually come a time when the cross-stream domain size is too small. Test simulations (with larger domains and discussed in detail in Redford *et al.* 2012) showed that wake widths up to ∼65 % of the domain size were not affected and in the results presented here the wake was always smaller than that limit. ('Wake width' here means twice the distance from the centreline to where the mean velocity has fallen to 1 % of its centreline value.) In addition, it was important to ensure a domain length sufficient to allow development of the largest axial structures. Figure 1(*b*) provides an example of the spatial correlation function of the axial velocity component, $R_x(\Delta)$, at the wake half-width point ($r = \delta$), when the local Re was ∼2000. $R_x(\Delta)$ is defined by

$$R_x(\Delta) = \frac{\overline{u_x[x/\Lambda_x]u_x[(x+\Delta)/\Lambda_x]}}{\overline{u_x\,(x/\Lambda_x)^2}}. \tag{2.1}$$

It is clear that the domain is more than adequate in that respect; its half-length is some 43 times the axial integral scale, computed as the area under the spatial correlation up to the first zero-crossing point. It was chosen to be so long in order to improve the data quality – recall the wake is axially homogeneous, so axial averaging could be employed to enhance statistical convergence.

Before presenting the basic data for both the self-similar wake (without external turbulence) and the HIT fields, we describe how the former was artificially combined with each of the latter. Each combination was implemented at a normalized time ($t = t_1 \approx 66$) when the pure wake had recovered from the very early response to the unphysical initial conditions and was approaching its self-similar state. Two constraints were used: the free-stream turbulence was inserted into the domain at all locations outside the mean wake (defined by the region in which the velocity was below 1 % of the centreline value) and at all places inside the mean wake where the turbulence kinetic energy (TKE) was smaller than 5 % of the maximum TKE inside the wake. Since the external turbulence flow fields were one quarter the length of the wake domain, and axially periodic, four identical turbulence fields were stacked axially. This is justified because the initial integral length scale of the turbulence field, L_{eo}, was in all cases small compared with the quarter-length domain, L_{dom} ($0.04 < L_{eo}/L_{dom} < 0.09$). Figure 2 illustrates the entire flow just after the two separate flows were combined; the axial stack of four external fields is clearly visible. Such fields (wake plus external turbulence) were then allowed to develop and decay with time and their features were analysed. We discuss first the two simulated base flows: the pure axisymmetric wake and the HIT.

3. The base flows

3.1. *The pure axisymmetric wake*

Johansson *et al.* (2003) suggested that the high-Reynolds-number similarity solution would not be expected to appear if the local Reynolds number ($Re = U_s\delta/\nu$) falls below ∼500, although in view of the Redford *et al.* (2012) conclusions, and since even at that Re the viscous terms are still small compared with the turbulence terms, this seems rather arbitrary. The latter authors also found that the existence of self-similarity does not rest on the existence of a clear inertial subrange in the energy spectrum.

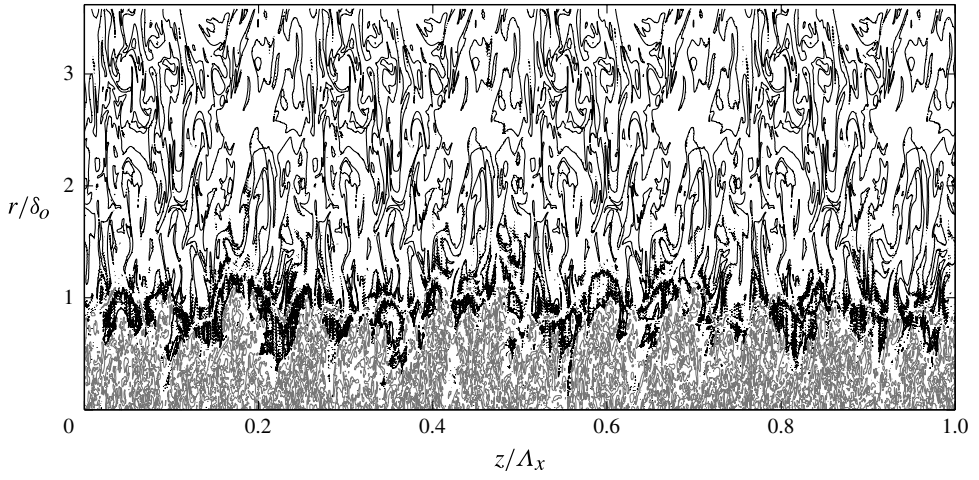

FIGURE 2. An example of the non-dimensional vorticity magnitude contours, $\widetilde{\omega} = \omega\delta_o/U_{so}$, immediately after the pure wake was artificially combined with the free-stream turbulence; grey: $\widetilde{\omega} = 12.8$ (the wake region) and black: $\widetilde{\omega} = 0.6$ (the external turbulence).

Figure 1 shows that in the present computations there is in fact a reasonable $-5/3$ range and figure 3(*a*) shows the variation of Re with time t. Note that t has (here and hereafter) been non-dimensionalized using the initial values of wake half-width δ_o and maximum velocity deficit U_{so}. Each variable was obtained at every time step by circumferential and axial averaging and, for clarity, only a small subset of the data is shown. After an initial development period (not shown, but prior to $t = 50$) Re remains above 1000 for the entire computation. The $n = 1/3$ solution predicts that both Re and Re_t will fall like $t^{-1/3}$. Taking the virtual origin to be $t_o = 50$ and choosing appropriate amplitudes yields the solid and dashed lines shown in the figure. Both Re and Re_t behave largely as expected beyond about $t \approx 125$. Likewise, the turbulence Reynolds number, defined by $Re_t = k^2/\epsilon\nu$, remains higher than 300. The $n = 1/3$ solution has turbulence stress values at fixed r/δ varying like $t^{-4/3}$. The three fluctuating (r.m.s.) velocities at the wake half-width ($r = \delta$) are appropriately plotted in figure 3(*b*) and it is clear that they demonstrate quite a good fit to the expected behaviour, again suggesting a virtual origin of about $t_o = 50$ using the data for $t > 125$. Data at the half-width location are used throughout this paper, since these inevitably have a much smaller level of statistical scatter. Recall that axial and circumferential averaging are used; the latter naturally contributes very little to reduction in statistical scatter for r close to zero.

The growth of the wake half-width and decay in centreline velocity are shown in figure 4(*a*), where values have been normalized by the initial values at $t = 0$. It is evident that good fits to the expected slopes in these log–log plots are observed at least over the period beyond $t \approx 125$. Note that the necessary similarity constraint $\delta^2 U_s$ is also closely satisfied. Figure 4(*b*) shows the variation of the r.m.s. velocities at $r = \delta$, normalized by U_s^2; these all become roughly constant for $t > \approx 125$, as they should in a self-similar region, where $\overline{u_x u_r}/U_s^2$ at fixed r/δ is constant (and similarly for the other stresses). Although choice of a smaller t_o would yield reasonable mean flow data fits (in figure 3) over an earlier time period, the r.m.s. data of figure 4(*b*) indicate that

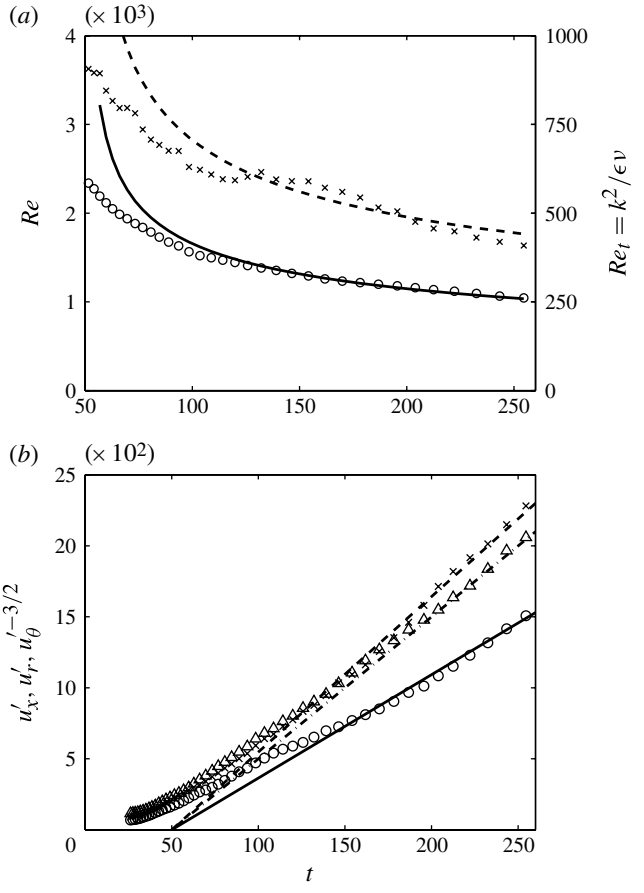

FIGURE 3. (*a*) Variations of Re ($\times$) and Re_t ($\circ$) with (normalized) time. (*b*) Un-normalized r.m.s. velocities at $r = \delta$: $\circ$, u'_x; $\triangle$, u'_r; $\times$, u'_θ. The lines are fits to the data over the $75 < t - t_o < 205$ period, with a virtual origin of $t \equiv t_o = 50$.

self-similarity is not closely achieved much earlier than $t \approx 125$. The velocity profile (not shown) was obtained by assuming similarity and averaging over $125 < t < 255$ and is very close to the cosinusoidal variation suggested to provide a reasonable fit by Ostowari & Page (1989). However, there is no fundamental reason why one should expect a cosinusoidal velocity variation – this would, for example, require a rather special variation of eddy viscosity if it were to arise naturally from the similarity form of the equations.

Turbulence quantities were also computed and the dimensionless Reynolds stress profiles are presented in figure 5(*a*). Individual profiles were obtained by appropriate circumferential and axial averaging and collapsed quite well for each time within the self-similar period ($t > 125$), so the profiles shown are those resulting from time-averaging over that period. They agree qualitatively with previously reported data (for example Uberoi & Freymuth 1970) but, as mentioned in § 1, quantitative agreement might not be expected unless sufficient time has elapsed (or downstream distance is great enough, in the spatial case). In fact, the profiles are quantitatively quite close

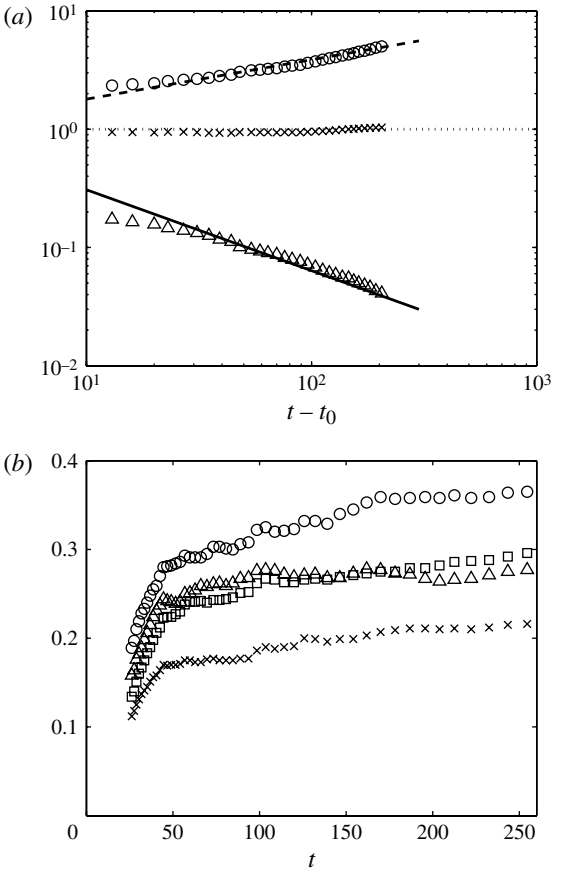

FIGURE 4. (*a*) Variation of wake half-width (∘) and maximum deficit velocity (△) with time; ×, $\delta^2 U_s/\delta_0^2 U_{so}$. The data are normalized by their initial values at $t = 0$, $\delta_o = 0.732$, $U_{so} = 0.505$. (*b*) r.m.s. velocities at $r = \delta$: ∘, u_x'/U_s; □, u_r'/U_s; △, u_θ'/U_s; ×, $\sqrt{\overline{u_x u_r}}/U_s$.

to the results of Redford *et al.* (2012), with peak r.m.s. levels not very different from those found by the latter in the genuinely self-similar regime.

Finally, once all the wake properties were extracted the TKE balance was calculated using the following equation:

$$\begin{aligned}
&\text{Convection} \quad \frac{\delta}{U_s^3}\frac{\partial\left[\frac{1}{2}\left(\overline{u_x^2}+\overline{u_r^2}+\overline{u_\theta^2}\right)\right]}{\partial t}\\
\text{Transport} \quad &+\frac{1}{r/\delta}\frac{\partial}{\partial\,(r/\delta)}\left\{\overline{\frac{r}{\delta}u_r\left[\frac{p}{\rho}+\frac{\frac{1}{2}\left(u_x^2+u_r^2+u_\theta^2\right)}{U_s^3}\right]}\right\}\\
&\text{Production} \quad -\frac{\overline{u_x u_r}}{U_s^2}\frac{\partial}{\partial\,(r/\delta)}\left(\frac{U}{U_s}\right)\\
&\text{Dissipation} \quad +15\nu\frac{\delta}{U_s^3}\overline{\left(\frac{\partial u_x}{\partial x}\right)^2}=0.
\end{aligned} \tag{3.1}$$

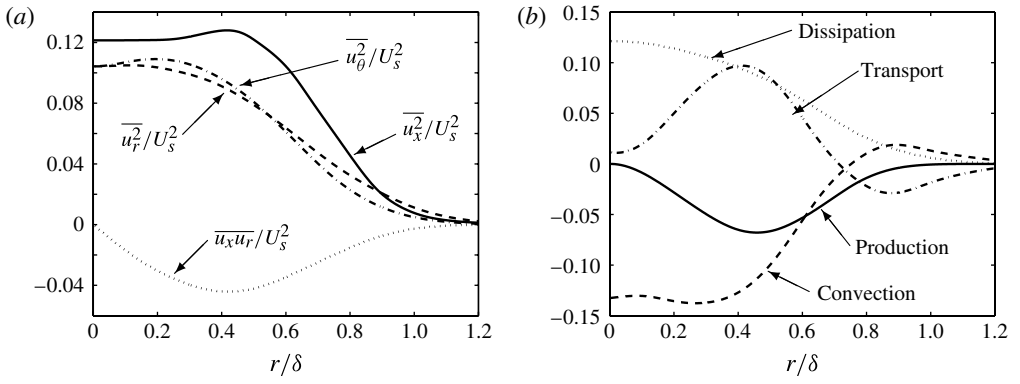

FIGURE 5. (*a*) Profiles of the dimensionless turbulent velocity fluctuations in the self-similar wake where u_z, u_r and u_θ are the fluctuating velocities in the x-, r- and θ-directions respectively and overbars refer to spatial averages. (*b*) Profiles of the various dimensionless components of the TKE balance in the self-similar wake.

Note that the boundary layer approximation has been used and, in computing the dissipation term (ϵ), local isotropy of the smallest scales of motion was assumed. The difference between the resulting value of ϵ and that obtained by using the exact expression was found to be negligible everywhere. Each term is normalized using the characteristic scales, U_s and δ. The data for the directly computed transport term (i.e. from gradients of triple velocity and pressure–velocity products) were found to be too scattered – an even longer domain would have been required to reduce the scatter. The transport term was therefore deduced as the balance from the other terms, as is often done in experimental studies, for just the same reasons (see Uberoi & Freymuth 1970, for example). Figure 5(*b*) shows the resulting TKE balance. Again, only qualitative agreement with the Uberoi & Freymuth (1970) wake is expected. Nonetheless, the absolute value of the ratios between the production and all the other terms at the wake half-width location are of order one, which is not much lower than those deduced from the Uberoi & Freymuth (1970) data.

We conclude that the computed wake, at least beyond $t \approx 125$, is satisfactorily self-similar with $n = 1/3$, yielding mean velocity, stress and TKE profiles quite similar to those previously reported. The Reynolds number is sufficiently high to yield isotropy of the smallest scales and around a decade of inertial subrange. At the end of this period $t = 255$, $Re = 1035$ and the Taylor-microscale Reynolds number $Re_\lambda = 104.6$ (deduced using $\lambda^2 = 2\overline{u_x^2}/\overline{(\partial u_x/\partial x)^2}$, Pope 2000). At $t = t_1$, $Re_\lambda = 130$. For all the computations discussed in § 4 the external turbulence was imposed at (normalized) $t = t_1 \approx 66$, slightly earlier than the start of the self-similar region. This allowed the unphysical behaviour arising from the combination process to die down, so that the resulting wakes beyond $t = 125$ could sensibly be compared with the pure-wake case.

3.2. *External turbulence*

Three different turbulent flow fields were generated. There have been many examples of HIT generated within a box by DNS (for example Rogallo 1981; Sullivan *et al.* 1994; Wang *et al.* 1996; Kaneda *et al.* 2003; Ishida, Davidson & Kaneda 2006) so we present only a brief discussion along with the basic data for the three cases.

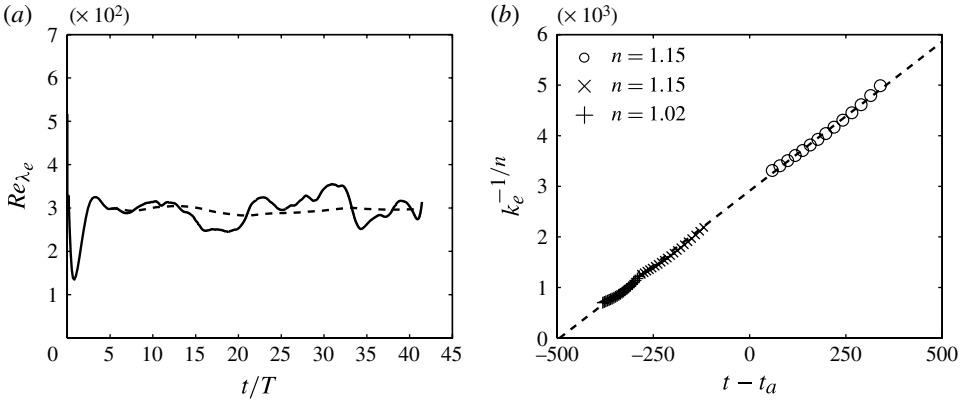

FIGURE 6. (*a*) Taylor microscale Reynolds number versus t/T for $u'_{eo}/U_{so} = 0.36$. Solid line: DNS result; dashed line: trace of the running average. (*b*) Decay of TKE ($k_e \sim t^{-n}$) in the external turbulence: ∘, weak; ×, medium; and +, strong turbulence cases.

Symbol	u'_{eo}/U_{so}	L_{eo}/δ_o	$\lambda_{eo}/\lambda_{\delta o}$	$\eta_{eo}/\eta_{\delta o}$	$T_{eo}/T_{\delta o}$	λ_{eo}/L_{eo}	η_{eo}/L_{eo}	Re_{λ_e}
∘	0.09	0.76	3.34	3.39	7.33	0.5	0.0187	133
×	0.17	0.52	1.9	1.84	2.6	0.41	0.0147	146
+	0.36	0.63	2.06	1.3	1.5	0.35	0.0085	314

TABLE 2. Defining parameters of the different external turbulence flow fields at t_1: λ_δ and λ_e are the Taylor microscale at the wake half-width location and in the external turbulence respectively; η_δ and η_e are the Kolmogorov scale η at the wake half-width location and in the external turbulence respectively; and $Re_{\lambda_e} = u'_e\lambda_e/\nu$ is the microscale Reynolds number in the external flow. L is the (axial) integral scale, suffix 'e' denotes values in the external turbulence and suffix 'o' denotes values at the time when the two flows are combined.

As mentioned in § 2, to achieve specific values of u'_{eo}/U_{so} Sullivan *et al.*'s (1994) forcing scheme was used and the computation proceeded until a fully quasi-stationary state was reached (as explained by Kaneda *et al.* 2003, for example). Figure 6(*a*) shows the time variation of Re_{λ_e} and its running average for the $u'_{eo}/U_{so} = 0.36$ case. Recall that here U_{so} is the base-line wake deficit velocity at t_1, the time at which the external turbulence field is added. (Suffix 'e' has its usual meaning, so that Re_{λ_e} denotes the Taylor-microscale Reynolds number $u'\lambda/\nu$ in this external turbulence field.) Note that the running average converges gradually to an approximately constant value such that additional simulations for $t/T > 30$, where $T = L_{eo}/u'_o$ is one eddy turnover time, showed little further change. Table 2 provides a summary of the turbulent characteristics of the three different HIT flow fields at t_1. The table shows that the range of external turbulence 'strengths', u'_{eo}/U_{so}, was from 0.09 to 0.36. For a corresponding spatially developing case of a wake in a turbulent free stream (velocity U_∞) and taking a centreline deficit velocity of around 10 % of the free-stream velocity, this range is roughly equivalent to $u'_e/U_\infty = 0.01$–0.04.

As soon as the external turbulence was artificially combined with the wake, its Sullivan *et al.* (1994) forcing was removed so that it was allowed to decay in the usual

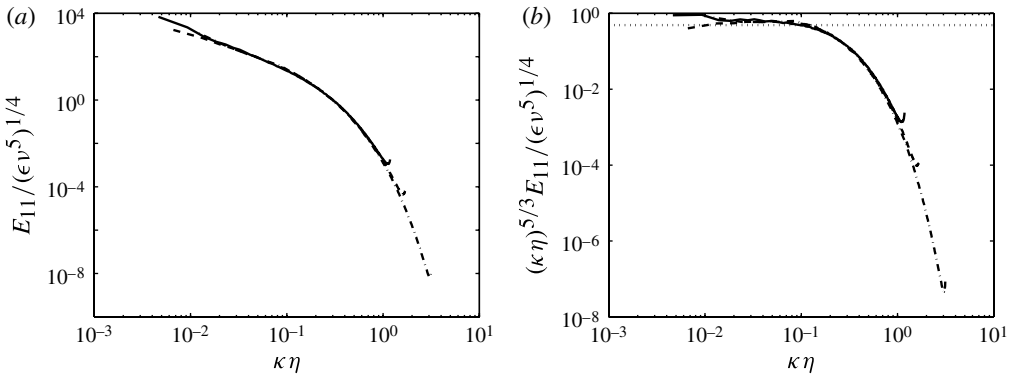

FIGURE 7. (*a*) Axial velocity one-dimensional energy spectrum and (*b*) the corresponding compensated spectra at $t = t_1$. Solid line: $u'_{eo}/U_{so} = 0.36$; dashed line: 0.17; dashed-dot line: 0.09; dotted line in (*b*) is the universal spectrum.

way. The nature of this decay was determined by interrogating the turbulence field *without* the combined wakes being present. As emphasized by Ishida *et al.* (2006), isotropic turbulence can decay either like Saffman's turbulence, $k_e \sim t^{-6/5}$ (where $k_e = (1/2)(\overline{u_x^2} + \overline{u_r^2} + \overline{u_\theta^2})$ is the TKE), or Batchelor's turbulence, $k_e \sim t^{-10/7}$, depending on initial conditions. For the former case $k_e L_e^3 =$ constant and our simulations yielded only small variations in this parameter with time whereas $k_e L_e^5$, the corresponding parameter which would be constant in Batchelor turbulence, actually rises significantly in all three cases. This suggests that our DNS turbulence is more Saffman-like, as also found by Krogstad & Davidson (2010) in their wind tunnel grid turbulence. They argue that if the constant A in the empirical decay law

$$\frac{\mathrm{d}\overline{u^2}}{\mathrm{d}t} = -A\frac{\overline{u^2}^{3/2}}{L_e} \tag{3.2}$$

falls with t like $A \sim t^{-q}$ Saffman turbulence would yield a decay exponent for $\overline{u^2} \sim t^{-n}$ of $n = 1.2(1-q)$ ($q \ll 1$). Our data do indeed show a slow (although rather scattered) fall in A with t and fits to the turbulence energy using $n = 1.15$ are reasonable, as shown in figure 6(*b*) and consistent with expectations (t_a in figure 6*b* is an appropriate virtual origin chosen for each case to allow collapse of all data to the same line). Note, however, that the strongest case requires an even smaller value of n, consistent with a faster drop in A.

Figure 7 shows axial velocity spectra for all three cases at $t = t_1$, plotted in the usual way to emphasize collapse in the inertial subrange and, more clearly in the compensated spectra of figure 7(*b*), the extent of this range. In all three cases the latter is comparable with the extent of the inertial range in the pure-wake spectrum (see figure 1*a*). Note that the range of (normalized) scales captured by the simulation is rather smaller for the higher energy cases, since the Kolmogorov scales are larger in those cases (see table 1).

We conclude that our three HIT fields show reasonable consistency and agreement with previously reported ones, but it is emphasized again that the influence of initial conditions can undoubtedly lead to different behaviour.

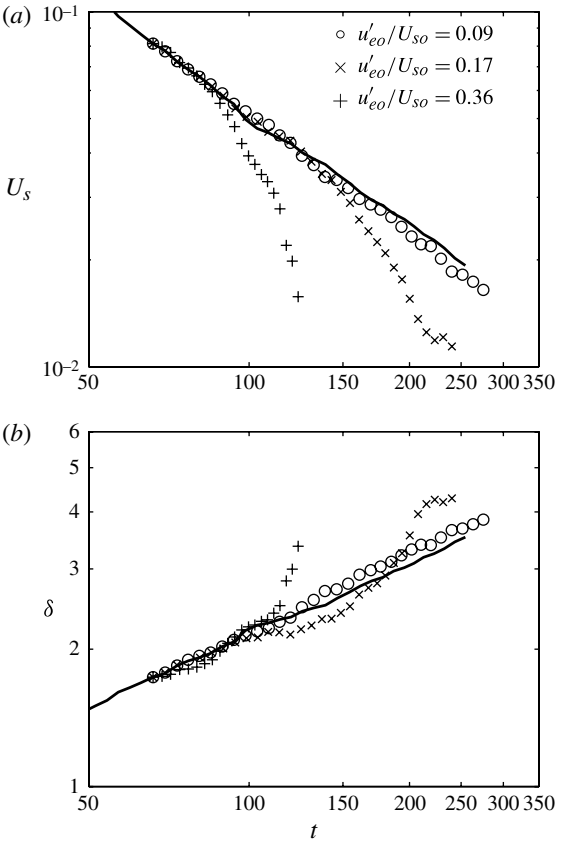

FIGURE 8. (*a*) Decay of deficit velocity, U_s. (*b*) Growth of wake half-width, δ. Solid line is the pure-wake case and the different values of u'_{eo}/U_{so}, see table 2, are shown in the legend.

4. The wake embedded in external turbulence

Once the pure wake and the turbulent flows were achieved separately they were artificially combined (as explained in § 2) and the whole field – wake plus external turbulence – was then allowed to develop and decay with time.

In the light of the discussion in § 1, the first anticipated feature is that the presence of free-stream turbulence will enhance the decay rate of the wake. Figure 8 shows the wake growth and corresponding decay of the centreline velocity. Recall that the external turbulence was in each case imposed at (normalized) $t = t_1 \approx 66$. It is immediately obvious that increasing levels of external turbulence cause substantial changes, although these appear to be small for the weakest turbulence case. Since it is not known *a priori* whether similarity is possible nor, even if it is, what the virtual origin would be for that region of the wake, it is not sensible to use log–log plots like these to deduce decay rates. Figure 9(*a*) shows the deficit velocity plotted as $U_s^{-1/2n}$ versus t for the three cases, compared with the pure-wake case. The value of n has been chosen in each case to yield reasonable straight lines after an initial adjustment region; these values are 0.33, 0.4 and 0.5 in the order of increasing u'_{eo}/U_{so} (see table 1), compared with 1/3 for the pure-wake case.

Note first from figure 9(*a*) that the wake decay rate for the weakest external turbulence case is not noticeably different from that of the pure wake, although

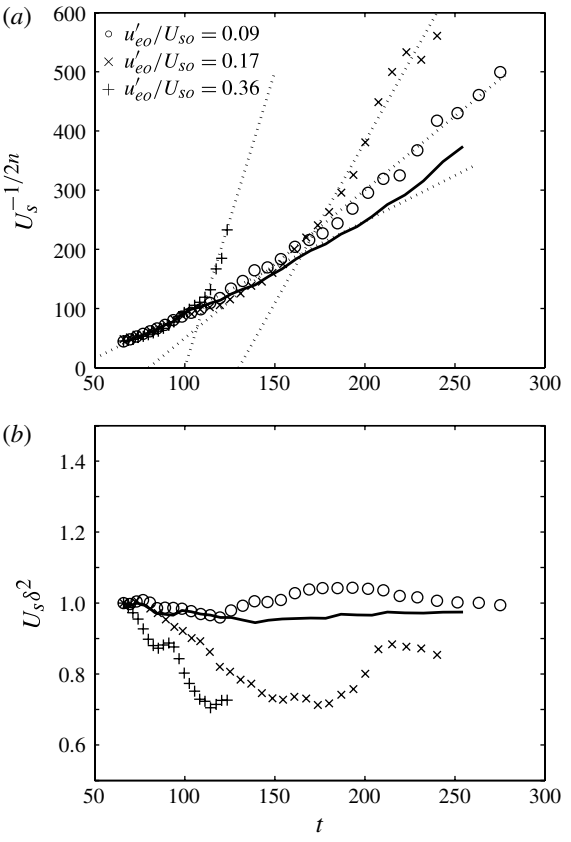

FIGURE 9. (*a*) Variation of $U_s^{-1/2n}$; solid line is the pure-wake case. Dotted lines have $n = 0.33$, 0.4 and 0.5 for the $u'_{eo}/U_{so} = 0.09$, 0.17 and 0.36 cases, respectively. (*b*) Variation of $U_s\delta^2$; lines and symbols as in (*a*).

the multiplying factor α in $U_s = \alpha t^{1/2n}$ is rather smaller. Secondly, however, the rate of decay thereafter increases significantly with increasing strength of the external turbulence. This is unlike the behaviour reported by Wu & Feath (1994) and Legendre *et al.* (2006) who each noticed only one decay rate ($U_s \approx x^{-1}$ and $U_s \approx x^{-2}$, respectively). But as discussed earlier, these cases had additional complications (like mean velocity shear external to the wake). Amoura *et al.* (2010) also found $U_s \approx x^{-2}$ but their external turbulence was very strong (see table 1). The present trend is in general agreement with the initial work of Redford & Coleman (2007). It is worth emphasizing that in determining decay rates one should recognise the likely non-zero value of a virtual origin. This makes detailed comparisons with the earlier literature problematic, because none of the authors listed in table 1 took any account of possible virtual origins, using plots like those in figure 8(*a*) to determine n.

Thirdly, it is also clear that the effect of the external turbulence does not take place instantaneously but is delayed by a time that tends to decrease with increasing u'_{eo}/U_{so}. By examining energy spectra it was found that the stronger the external turbulence, the longer the initial correction stage was but in all three cases it was shorter than 20 time units. So the correction stage presumably has little influence on the time taken to affect the decay rate. Note that the correction stage, which evolves as a result of

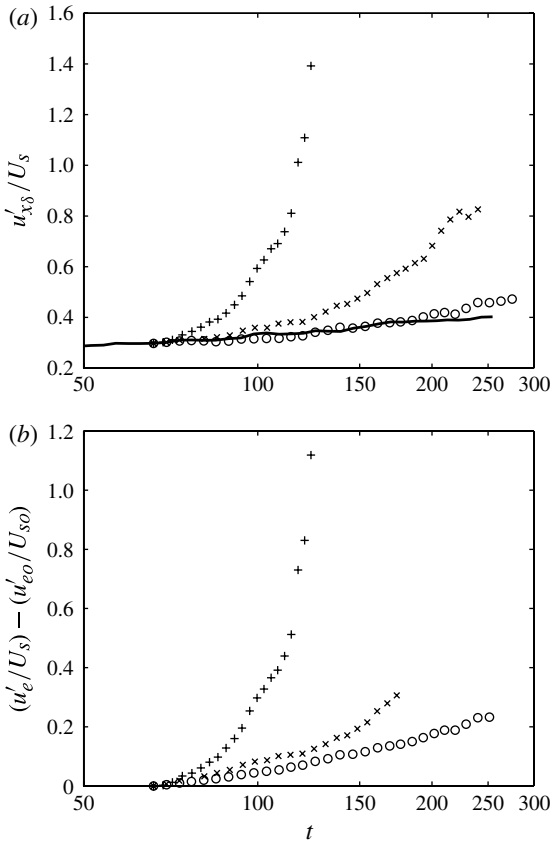

FIGURE 10. (*a*) u'_{x_δ}/U_s versus time; line and symbols as in figure 9. (*b*) The change in u'_e/U_s versus time for the different wake–background combinations; lines and symbols as in figure 8.

the artificial 'wake plus free stream' assemblage, was typified by, for example, energy spectra containing unphysical peaks, but this stage has no physical significance and is not explored here.

Although a reasonable power-law fit to $U_s \sim (t - t_o)^{-2n}$ seems possible in every case, figure 9(*b*) demonstrates that self-similarity does not hold even approximately, at least for the two stronger turbulence cases, since $U_s\delta^2$ is far from constant. (This parameter is only constant on the self-similar assumption that $U = U_s f(\eta)$, $\eta = r/\delta$.) Moreover, neither mean velocity nor turbulence profiles can be collapsed in self-similar form (see later). Figure 9(*b*) suggests, however, that in the weakest external turbulence case, the wake may not be very far from a self-similar form, at least in terms of its mean velocity behaviour, since $U_s\delta^2$ remains constant within $\sim \pm 4\,\%$.

The time variation of the ratio u'_{x_δ}/U_s, where u'_{x_δ} is the r.m.s. axial velocity at the wake half-width location, is shown in figure 10(*a*). Notice again that the divergence from the pure-wake data (for which the ratio is approximately constant) is increasingly more rapid and larger as u'_{eo}/U_{so} increases. Recall that an early idea in considering these flows was that since the pure-wake decay in U_s/U_∞ occurs at about the same rate as the HIT decay of u'_e/U_∞, perhaps the controlling parameter u'_e/U_s in the combined case may be roughly constant. However, our data show very different

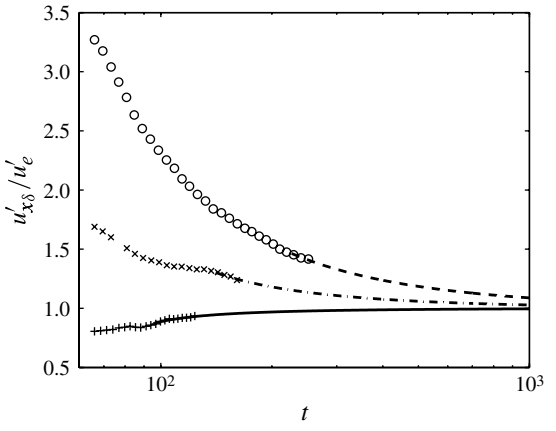

FIGURE 11. Variation with time of the ratio of axial intensity in the wake (at $r = \delta$) to free-stream intensity; symbols as in figure 8 and the lines are plausible extrapolations towards the final state $u'_{x\delta} = u'_e$.

behaviour, as illustrated in figure 10(*b*): in the presence of external turbulence, the decay of the wake centreline deficit velocity is significantly faster than the natural decay in the free-stream turbulence intensity, so u'_e/U_s in fact continually rises with time. The behaviour is emphasized in figure 11, which shows that the ratio of the half-width axial turbulence intensity, $u'_{x\delta}$, to the free-stream intensity, u'_e, continually falls (or, in the case of $u'_{eo}/U_{so} = 0.37$ initially, rises) towards what must be the eventual state in which $u'_{x\delta} = u'_e$. Since the wake r.m.s. velocity profiles must eventually be determined by the background, which is decaying relatively slower, no self-similar state can be achieved.

The non-dimensional profiles of the different turbulence stresses were also examined. They change with time, each from its original self-similar profile into one which is more closely uniform and clearly determined by the external turbulence intensity – higher values of u'_{eo}/U_{so} lead to more rapid and larger effects, as noted earlier; examples are presented in figure 12. Notice that the shear stress (figure 12*a,c*), when normalized using the centreline velocity deficit, grows (in magnitude) rather than decays with time. This might at first seem something of a surprise, as one might suppose that the external turbulence would tend to make the wake turbulence more isotropic and hence reduce the Reynolds shear stress. However, the production term in the transport equation for the shear stress is $\overline{u'_r{}^2}\partial U_r/\partial r$ (normalized using U_s and δ) and, like the axial stress shown in figure 12(*b,d*), $\overline{u'_r{}^2}$ rises significantly with time. The maximum mean shear is relatively less affected so production of Reynolds shear stress is rapidly enhanced by the external turbulence. This cannot continue for ever, however; eventually, the mean flow deficit profile will become sufficiently 'eaten away' by the external turbulence that it will essentially collapse, although recall that the wake volume flux must remain constant. This will cut off the source of shear stress production so that the latter must eventually also decay. The present computations did not extend sufficiently in time to reach that point.

Nonetheless, since the non-dimensional r.m.s. velocity profiles develop with time to ones which are eventually determined by their values in the (isotropic) free stream, the turbulence normal stress profiles inside the wake must eventually become more equal and uniform, at least for the two strongest cases. The $\overline{u'_x{}^2}$ data in figure 12(*b,d*) have

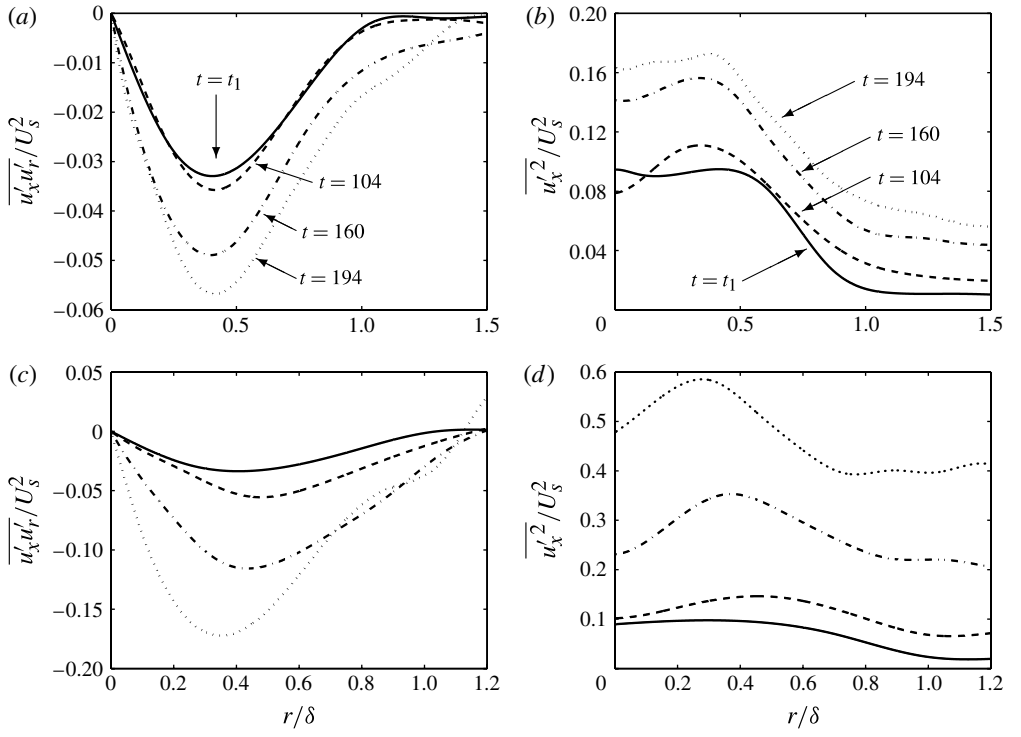

FIGURE 12. Profiles of $\overline{u'_x u'_r}/U_s^2$ at different times for (*a*) $u'_{eo}/U_{so} = 0.09$, (*c*) 0.17 initially. Profiles of $\overline{u'^2_x}/U_s^2$ at different times for (*b*) $u'_{eo}/U_{so} = 0.09$, (*d*) 0.17 initially. Line types in (*c,d*) have the same t as those in (*a,b*). Note the different ordinate scales in (*a,c*), and in (*b,d*).

this feature. Overall, the external turbulence drives an evolution of the wake turbulence away from its initial self-similar state towards the (decaying) state of the external turbulence. This behaviour can be further illustrated by considering the development of the stress anisotropy tensor (Pope 2000). Formulating the computed stresses in terms of the second and third invariants of that tensor in the usual way and plotting in the form of the 'Lumley triangle' leads, for the $u'_{es}/U_{so} = 0.09$ and 0.36 cases, to the results shown in figure 13. At $t = t_1$ the wake data (the square) lie within the region containing all the pure-wake data, but as time progress the $\xi - \eta$ point moves out of this region and eventually (the triangle) lies within the external turbulence regime, not far from the exact isotropy point on the map, $\xi = \eta = 0$.

We comment finally on the possible influence of the initial scale ratio, L_{eo}/δ_o. This varied only weakly through the three cases, although the variation was non-monotonic, with the smallest value (0.52) occurring for the medium-strength turbulence case, $u'_{eo}/U_{so} = 0.17$ (see table 2), and the values were all $O(1)$. Such values might be expected to lead to more significant effects on the wake than would be the case for either very large ($\gg 1$) or very small ($\ll 1$) scale ratios. For the former one might expect that the initial first-order effect of external turbulence would be to 'shake' the wake around whereas for the latter it would simply 'nibble' very slowly at the edges of the wake. In the present case, as the wake develops the local ratio L_e/δ falls. For the $u'_{es}/U_{so} = 0.09$ case the fall is from 0.75 to 0.4 over the time range of the computation, whereas it is 0.52 to 0.43 and 0.63 to 0.33 for the $u'_{es}/U_{so} = 0.17$ and

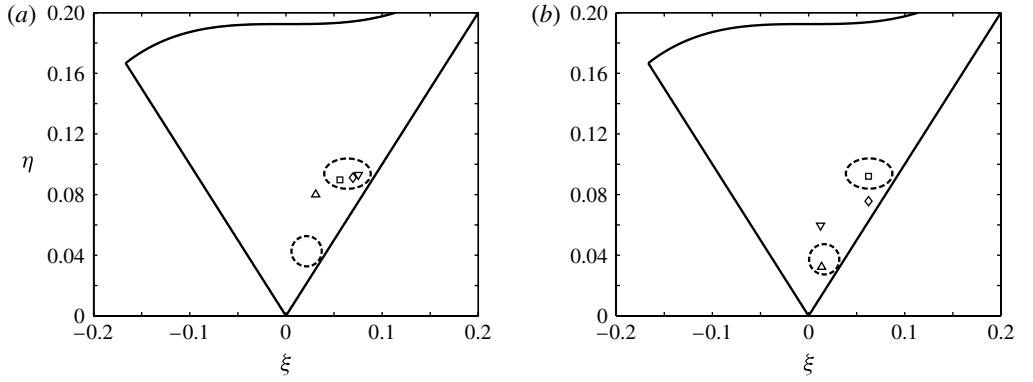

FIGURE 13. The Lumley triangle (solid lines) on the plane of the invariants ξ and η of the Reynolds-stress anisotropy tensor. Development in time of the turbulence. (*a*) The $u'_{es}/U_{so} = 0.09$ case; $t =$: □, t_1; ◇, 132; ▽, 202; △, 275. (*b*) The $u'_{es}/U_{so} = 0.36$ case; $t =$: □, t_1; ◇, 94; ▽, 112; △, 130. The dashed circles contain the external turbulence data over the entire period and the dashed ellipses contains the self-similar (pure) wake data.

0.36 cases, respectively. Compared with the changes with time in u'_e/U_s (figure 10) these are quite small variations and it seems very likely that it is the latter parameter which has the major controlling influence on the developing wake, at least for the present cases for which $L_e/\delta = O(1)$. It is likely that larger variations in L_{eo}/δ_o between the three cases for, say, the same values of u'_{es}/U_{so} would lead to noticeable (and separable) effects of the former, but such cases have not been studied. In the context of wall boundary layers in the presence of external turbulence Hancock & Bradshaw (1989) have shown that both parameters can have significant effects and, as noted above, this seems intuitively likely for free shear flows also. Recall that due to the way in which the external turbulence was generated in the present case, the initial integral length scale could not be specified *a priori*. However, it would be possible to embed significantly smaller wakes into such fields (so that L_{eo}/δ_o is higher) and this may be a fruitful avenue of further work, although to extend the range of L_{eo}/δ_o very significantly would probably require greater computational resources.

5. Final remarks and conclusions

Time-developing axisymmetric wakes embedded in external turbulence have been studied using DNS. In spite of the inherent limitations of the method, it has been shown first that our pure wake (no external turbulence) is comparable to previously reported spatially developing far axisymmetric wakes in uniform free streams and that the external turbulence is very similar to the Saffman-type HIT generated by previous authors. The self-similar wake was inserted into three HIT fields and allowed to develop with time. Our chosen distinguishing parameter between the three resulting wake cases was u'_{es}/U_{so}, the ratio of the external turbulence intensity to the wake centreline velocity deficit at the moment the external turbulence was added. This varied from 0.09 to 0.36, representing relatively weak to significantly stronger external turbulence and is equivalent roughly to a range of 0.01–0.04 in the ratio of free-stream intensity to free-stream mean velocity, u'_e/U_∞, in a typical corresponding case of a spatially developing flow (for a wake whose maximum velocity deficit is around 10 % of the free-stream mean velocity). So none of the cases studied here has as strong an initial external turbulence as that studied by Amoura *et al.* (2010). In all three

cases the initial ratio of the integral scale in the external turbulence to the wake width, L_{eo}/δ_o, was in the range 0.5–0.75 and did not change very significantly during the subsequent development of the wake and the external turbulence; this is quite similar to the values in the spatially developing case of Amoura *et al.* (2010). The more rapid decays found in the latter studies compared with those found here (albeit with the uncertainty regarding possible effects of virtual origins, mentioned earlier) are therefore probably caused by the much stronger external turbulence, although recall too that the Amoura *et al.* (2010) wakes developed in axially homogeneous turbulence. Unlike previous work, the wakes studied here are embedded within decaying external turbulence. But despite similar decay rates of this turbulence and the pure wake, it seems clear that external turbulence enhances the wake decay rate increasingly rapidly as u'_{eo}/U_{so} rises, so that (apparent) power laws have an increasing value of the exponent n (from the classical pure-wake value of $1/3$). This is all in the context of cases for which the integral length scale of the external turbulence is initially of the same order as that of the wake.

The major conclusion of the present work is that even though power-law decay may seem to occur, any possibility of self-similarity in the developing wake is destroyed by the action of the external turbulence. This suggests that there is in fact no reason in principle to anticipate a fixed (for each case) power-law behaviour in the decay of centreline deficit velocity or growth in wake width. The turbulence structure inside the wake evolves from its initial self-similar state towards the state of the external turbulence, with the normal Reynolds stresses becoming progressively more uniform across the wake. This happens gradually, starting at the wake edges and, like the wall boundary layer case discussed by Hancock & Bradshaw (1989), is probably driven primarily by the influence of fluctuating strain rates in the external flow on the outer part of the wake, through the intermittent ingestion of the external fluid into the wake. Although typical wake shear stresses initially increase in magnitude (because the relevant shear stress production term in its transport equation increases) they must eventually decay along with the mean flow profile, consistent with a complete collapse of the wake towards the state of the external turbulence. It has not been possible, however, to explore the details of this final collapse.

Acknowledgements

We would like to acknowledge the School of Engineering Sciences at the University of Southampton for funding one of us (E.R.) via a research scholarship. We also thank the UK Turbulence Consortium, UKTC, for providing us with computer time on the UK EPSRC HPCx IBM supercomputer under EPSRC grant number EP/D044073/1. Finally, we would like to express our great gratitude to Professor G. Coleman and Drs J. Redford and R. Johnstone for their very helpful input throughout numerous discussions.

REFERENCES

AMOURA, Z., ROIG, V., RISSO, F. & BILLET, A.-M. 2010 Attenuation of the wake of a sphere in an intense incident turbulence with large length scales. *Phys. Fluids* **22**, 055105.

BAGCHI, P. & BALACHANDAR, S. 2003 Effect of turbulence on the drag and lift of a particle. *Phys. Fluids* **15**, 3496–3513.

BAGCHI, P. & BALACHANDAR, S. 2004 Response of the wake of an isolated particle to an isotropic turbulent flow. *J. Fluid Mech.* **518**, 95–123.

BATCHELOR, G. K. 1967 *An Introduction to Fluid Dynamics*. Cambridge University Press.

BEVILAQUA, P. M. & LYKOUDIS, P. S. 1978 Turbulence memory in self preserving wakes. *J. Fluid Mech.* **89**, 589–606.

CHEVRAY, R. 1968 The turbulent wake of a body or revolution. *Trans. ASME: J. Basic Engng* 275–284.

EAMES, I., JOHNSON, P. B., ROIG, V. & RISSO, F. 2011 Effect of turbulence on the downstream velocity deficit of a rigid sphere. *Phys. Fluids* **23**, 095103.

GEORGE, W. K. 1989 The self-preservation of turbulent flows and its relation to initial conditions and coherent structure. In *Advances in Turbulence* (ed. W.K. George & R. Arndt), pp. 39–73. Hemisphere.

GOURLAY, M. J., ARENDT, S. C., FRITTS, D. C. & WERNE, J. 2001 Numerical modelling of initially turbulent wakes with net momentum. *Phys. Fluids* **13** (12), 3783–3802.

HANCOCK, P. E. & BRADSHAW, P. 1989 Turbulence structure of a boundary layer beneath a turbulent free stream. *J. Fluid Mech.* **205**, 45–76.

ISHIDA, T., DAVIDSON, P. A. & KANEDA, Y. 2006 On the decay of isotropic turbulence. *J. Fluid Mech.* **564**, 455–475.

JOHANSSON, P. B. V., GEORGE, W. K. & GOURLAY, M. J. 2003 Equilibrium similarity, effects of initial conditions and local Reynolds number on the axisymmetric wake. *Phys. Fluids* **15** (3), 603–617.

KANEDA, Y., ISHIHARA, T., YOKOKAWA, M., ITAKURA, K. & UNO, A. 2003 Energy dissipation rate and energy spectrum in high resolution direct numerical simulations of turbulence in a periodic box. *Phys. Fluids* **15** (2), L21–L24.

KIM, J., MOIN, P. & MOSER, R. 1987 Turbulence statistics in fully developed channel flow at low Reynolds number. *J. Fluid Mech.* **177**, 133–166.

KROGSTAD, P.-A. & DAVIDSON, P. A. 2010 Is grid turbulence Saffman turbulence? *J. Fluid Mech.* **642**, 373–394.

LEGENDRE, D., MERLE, A. & MAGNAUDET, J. 2006 Wake of a spherical bubble or a solid sphere set fixed in a turbulent environment. *Phys. Fluids* **18**, 048102.

MOSER, R. D., ROGERS, M. M. & EWING, D. W. 1998 Self-similarity of time-evolving plane wakes. *J. Fluid Mech.* **367**, 255–289.

OSTOWARI, C. & PAGE, R. H. 1989 Velocity defect of axisymmetric wakes. *Exp. Fluids* **7**, 284–285.

POPE, S. B. 2000 *Turbulent Flows*. Cambridge University Press.

PRESS, W. H., FLANNERY, B. P., TEUKOLSKY, S. A. & VETTERLING, W. T. 1992 *Numerical Recipes in FORTRAN 77: The Art of Scientific Computing*. Cambridge University Press.

REDFORD, J. A., CASTRO, I. P. & COLEMAN, G. N. 2012 On the universality of turbulent axisymmetric wakes. *J. Fluid Mech.* **710**, 419–452.

REDFORD, J. A. & COLEMAN, G. N. 2007 Numerical study of turbulent wakes in background turbulence. *5th International Symposium on Turbulence and Shear Flow Phenomena (TSFP-5 Conference), Munich Germany*, pp. 561–566.

RIND, E. & CASTRO, I. P. 2012 On the effects of free stream turbulent on axisymmetric disc wakes. *Exp. Fluids* **53**, 301–318.

ROGALLO, R. S. 1981 Numerical experiments in homogeneous turbulence. *NASA Tech. Mem.* 81315.

SULLIVAN, N. P., MAHALINGAM, S. & KERR, R. 1994 Deterministic forcing of homogeneous isotropic turbulence. *Phys. Fluids* **6**, 1612–1614.

TOWNSEND, A. A. 1976 *Structure of Turbulent Shear Flow*. Cambridge University Press.

UBEROI, M. S. & FREYMUTH, P. 1970 Turbulent energy balance and spectra of the axisymmetric wake. *Phys. Fluids* **13** (9), 2205–2210.

WANG, L.-P., CHEN, S., BRASSEUR, J. G. & WYNGAARD, J. C. 1996 Examination of hypotheses in the Kolmogorov refined turbulence theory through high-resolution simulations. Part 1. Velocity field. *J. Fluid Mech.* **309**, 113–156.

WU, J.-S. & FEATH, G. M. 1994 Sphere wakes at moderate Reynolds numbers in a turbulent environment. *AIAA J.* **32** (3), 535–541.

WU, J.-S. & FEATH, G. M. 1995 Effect of ambient turbulence intensity on sphere wakes at intermediate Reynolds numbers. *AIAA J.* **33** (1), 171–173.

WYGNANSKI, I., CHAMPAGNE, F. & MARASLI, B. 1986 On the large-scale structure in two-dimensional small-deficit turbulent wakes. *J. Fluid Mech.* **168**, 31–71.

XIE, Z.-T. & CASTRO, I. P. 2008 Efficient generation of inflow conditions for large eddy simulation of street-scale flows. *Flow Turbul. Combust.* **81** (3), 449–470.